Proc. of the European Safety and Reliability Conference (ESREL 2026)
Edited by José C. Matos, Paulo B. Lourenço, Michael Beer, Daniel Oliveira,
Edoardo Patelli, Hélder S. Sousa, Rui A. Silva and Monica Santamaria

doi: 10.3850/ESREL2026061419_esrel26-p28977-cd

Development of a Sensor Density Reduction Methodology for Thermal Monitoring of Electronic Systems

Matteo Bertone
Dept. of Mechanical and Aerospace Engr., Politecnico di Torino, Italy. E-mail: matteo.bertone@polito.it

Giorgia Castorina
Dept. of Mechanical and Aerospace Engr., Politecnico di Torino, Italy. E-mail: s320007@studenti.polito.it

Paolo Maggiore
Dept. of Mechanical and Aerospace Engr., Politecnico di Torino, Italy. E-mail: paolo.maggiore@polito.it

Matteo D.L. Dalla Vedova
Dept. of Mechanical and Aerospace Engr., Politecnico di Torino, Italy. E-mail: matteo.dallavedova@polito.it

This paper presents a preliminary methodology for identifying and localizing anomalous heat sources on 2D surfaces in electronic systems using sparse sensor networks. As power densities in modern electronics continue to rise, effective thermal monitoring has become essential for preventing failures and ensuring long-term reliability. However, dense sensor deployment is often impractical due to cost constraints and spatial limitations. The proposed approach leverages heat-diffusion physics to predict the expected response of the sensor network to anomalies occurring at predetermined locations of interest. In this way, the computationally intensive simulation stage is decoupled from the real-time identification process, substantially reducing the monitoring system's computational burden. Experimental validation shows that, even with a 50-fold reduction in sensor count (a 98% decrease), the worst-case localization error increases only by a factor of 25. By enabling more cost-effective monitoring network deployments, the methodology supports the acquisition of detailed information about component operating conditions without interfering with primary system functions.

Keywords: PCB thermal monitoring, heat source localization, sparse sensor networks, electronic systems reliability.

1. Introduction

The power density of electronic systems has increased significantly in recent years, as illustrated in Fig. 1, and despite growing questions about Moore's Law as demonstrated by Kish (2002), it is expected to continue improving, as described by Theis and Wong (2017). Recent years have witnessed the widespread adoption of electrical systems even in applications not traditionally performed by electrical systems. Examples of such sectors include the extensive diffusion of electric vehicles in the automotive industry (as shown by Rajashekara (2013) and Fluchs (2020)) and the adoption of the more-electric philosophy in the aerospace sector (as shown by Buticchi et al. (2022)). Applications in these emerging sectors, while made possible by the newly achievable power densities, present numerous challenges in terms of component safety and reliability.

A consequence of the high power densities employed is the natural increase in temperatures

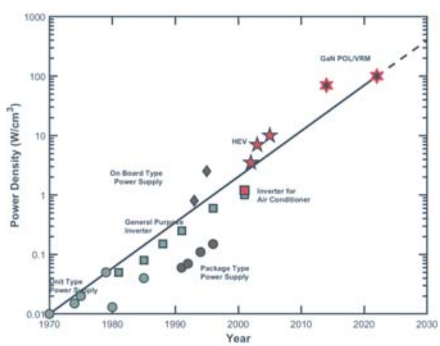

Fig. 1. Evolution of power density over time. Data from Saito (2023).

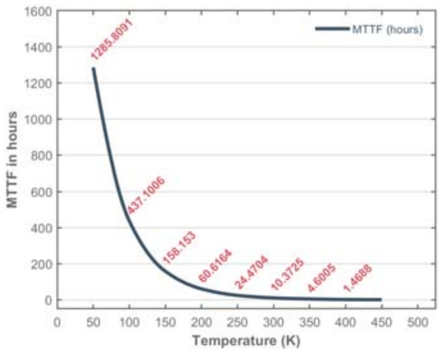

Fig. 2. Evolution of Mean Time To Failure as a function of temperature, as illustrated by Lakshminarayanan and Sriraam (2014).

that can be generated during operation. Monitoring and controlling these temperatures is critical in such systems, particularly because, as highlighted by Lakshminarayanan and Sriraam (2014) and shown in Fig. 2, many failure mechanisms in electrical systems are temperature-dependent, and consequently their operational lifetime is also affected.

Thermal monitoring of individual components therefore becomes important to ensure adequate operational lifetime. Unfortunately, individually monitoring every component installed in an electronic system or on a printed circuit board (PCB) is complex. Embedded temperature sensing within electrical components is achievable as demonstrated by Meijer et al. (2018), however, this integration approach is technically complex and not readily accessible, particularly for post-deployment diagnostic applications. In this context, deploying a limited sensor network capable of identifying anomalous hot spots represents a useful tool. During operation, it enables adaptation of operating conditions in response to localized thermal peaks. During fault identification phases, it facilitates the detection of potential short circuits. Furthermore, using a limited number of sensors minimizes system impact, allowing dedicated sensors as depicted by Kalker et al. (2021) to be reserved for only the most critical components while maintaining a general overview of system behavior.

2. Algorithm Description

Given the difficulty often associated with implementing sufficiently dense sensor networks, knowledge of the system's response to a particular phenomenon of interest within the domain under analysis enables the acquisition of additional information about the system behavior. In this context, the predominantly two-dimensional nature of PCBs facilitates the analysis of temperature diffusion across the entire PCB, as diffusion through the thickness is limited both by the material properties (typically fiberglass) and by the small thickness (typically less than 1.6 mm). In order to validate the proposed algorithm, and given the complexity associated with designing a dedicated PCB, a square homogeneous domain was chosen as the test sample. Although this configuration constitutes a simplification with respect to the complex trace topology of real circuits, it offers a reasonable approximation of PCBs featuring large copper fill regions.

With the analysis domain fully characterized, the system response to a thermal perturbation induced by abnormal component overheating is governed by the heat diffusion equation. Assuming a unit increase at the thermal source, the equation becomes:

$$T(r,t) = \frac{1}{4\pi\alpha t}\, e^{-\frac{r^2}{4\alpha t}} \tag{1}$$

where T denotes the temperature measured by the sensor, α represents the thermal diffusivity coefficient, r is the radial distance between the heat source and the sensor location, and t is the time elapsed between the onset of the temperature variation and the measurement acquisition. From this equation, it is possible to determine the precise response at each sensor, provided a waiting time is allowed for thermal perturbation diffusion. The selection of this temporal parameter, however, depends critically on both the dimensions of the surface under monitoring and the target spatial resolution. For constant spatial dimensions, extended waiting periods enable enhanced spatial resolution, whereas for constant waiting times, reduced spatial dimensions yield improved resolution.

Given the significant configurational degrees of freedom in the system under analysis, a sensor placement strategy was adopted whereby sensors are located at the centers of five identical circles that are mutually tangent and tangent to the domain boundary (see Fig. 4). This geometric arrangement minimizes the maximum source-to-sensor distance, enhancing thermal response characteristics, while maintaining unobstructed perimeter regions (typically allocated for connector placement) and contiguous areas for mounting components with larger footprints. Regarding the placement of heat sources representing individual components, in the absence of specific constraints, they were positioned at the nodes of a 16 × 16 grid. Each individual node therefore represents the source of the disturbance that induces the temperature variation measured by the previously positioned sensors. By simulating sensor readings for every grid position, a response matrix is obtained that characterizes the measurement network behavior for each individual "component" location. To facilitate direct comparison between simulated and experimentally measured results during system operation, the sensor temperatures obtained from each simulation were normalized. During the monitoring phase, the system calculates the discrepancy between the normalized temperature values measured by the sensors and those predicted by the simulations. The simulation yielding the minimum error identifies the component responsible for the thermal anomaly.

3. Experimental Assessment

To verify the adopted algorithms, a setup was developed in which the position of the heat source could be easily modified while keeping the sensor network unchanged. For the positioning of the heat source, 25 points distributed throughout the test field were selected.

3.1. *Experimental setup*

The overall architecture of the setup is comprised of three sections: the temperature monitoring system, the heat source control unit, and the test domain.

The temperature monitoring segment consists of a network of 5 temperature sensors positioned at the centers of circles that are simultaneously tangent to each other and to the edges of the test domain, together with their respective data acquisition and signal conditioning equipment.

The validation domain consists of a 50 mm × 50 mm × 2 mm square aluminum alloy plate. In order to limit disturbances caused by unknown external thermal sources, an insulating thermal enclosure was constructed to contain the plate during testing. The external housing also facilitates heat source positioning and provides mounting support for the heating element.

The heat source segment comprises a heating cartridge controlled via open-loop Pulse Width Modulation (PWM) to achieve maximum temperature stability. The inclusion of a Power Control Board allows both adjustable temperature control and the capability to power multiple heating cartridges.

Before proceeding with the experimental campaign, an analysis was necessary to determine the

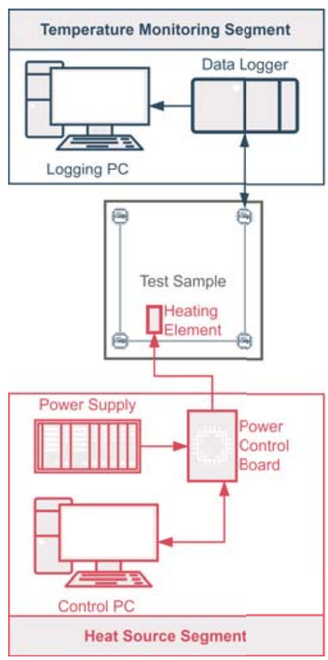

Fig. 3. Overall architecture of the experimental setup, illustrating the anomalous heat source segment and the measurement network.

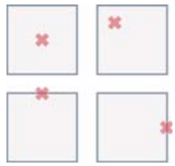

Fig. 4. Uncertainty-prone locations of the cells.

most appropriate waiting time for the experimental setup. Given the reasonable dimensions of the test sample and the limited temperature variations inducible by the heating elements, the waiting time was varied over a range from 5 s to 500 s. Based on analysis of the responses, a compromise value of 117 s was adopted to balance resolution and responsiveness.

3.2. *Experimental campaign*

For the algorithm verification, 25 points were selected to test the algorithm's performance under both ideal conditions (with the heat source positioned exactly at a grid node) and off-nominal conditions. Specifically, the point distribution was organized as follows:

- 20 measurement points randomly distributed within the domain to be uniformly spaced from the sensors.
- 4 measurement points positioned at the locations of the cells subject to the highest uncertainty (defined by the grid nodes; see Fig. 4).
- 1 measurement point positioned exactly at a sensor location.

As temperature control is implemented through open-loop PWM, various tests were carried out to determine optimal duty cycle values. Based on this preliminary analysis, a 55% duty cycle was chosen as a compromise between maintaining the thermal limits of the insulation materials and ensuring the sensor network's sensitivity to the induced temperature variations.

Finally, with respect to test duration, 25 minutes was selected to ensure adequate thermal diffusion that could be perceived even by the sensors most distant from the heat source.

4. Results Analysis

To evaluate the ability to correctly identify the heat source position, the algorithm was executed using the data obtained from the selected measurement points as input.

For the different points analyzed, the position error between the algorithm-estimated value and the actual value was calculated as a percentage with respect to the characteristic dimension of the validation domain, which in this case is the plate side length. Additionally, to evaluate effectiveness compared to direct sensor placement near the heat source, the error ratio at different measurement points relative to this reference condition was calculated. The results of this analysis are presented in Table 1.

Observation of Table 1 reveals a mean error of 24.43%. Analysis of the percentage error as a function of measurement point position shows that the highest errors occur at points located near the test sample boundaries. Given the geometry of the thermal enclosure, these zones are susceptible to minor thermal exchange with the external environment. These errors are therefore partially explained by the inherent characteristics of the experimental setup utilized for validation.

To evaluate not only the algorithm's ability to correctly identify the source location but also the stability of the estimated values, the extent of the area identified as a ”region of interest” was assessed. This region is defined as the area

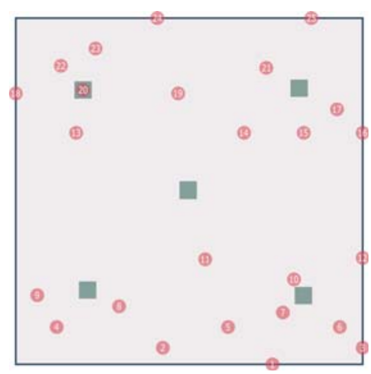

Fig. 5. Arrangement of sensors (green squares) and measurement points (red circles) with their respective identification numbers.

Table 1. Heat source localization performance across different measurement points.

Measurement Point	Error (%)	Relative Error
1	50.01	23
2	7.82	4
3	20.08	9
4	34.10	16
5	13.74	6
6	37.43	17
7	16.94	8
8	15.28	7
9	12.89	6
10	20.49	10
11	24.76	12
12	25.66	12
13	34.06	16
14	3.54	2
15	39.02	18
16	46.08	21
17	26.43	12
18	40.60	19
19	46.11	21
20	2.15	1
21	16.53	8
22	19.75	9
23	10.82	5
24	19.04	9
25	26.42	12

Note: The error is calculated as a percentage of the characteristic dimension of the test sample.

Note: The relative error is calculated with respect to the optimal positioning scenario, in which the heat source is located exactly at the sensor position, as represented by measurement point 20.

Table 2. Area in which points exhibit an error between the model-estimated and measured temperature distribution on the sensors of less than 10%.

Measurement Point	Relative Area (%)
1	3.24
2	2.73
3	8.15
4	19.36
5	9.54
6	2.84
7	9.32
8	17.30
9	17.80
10	7.81
11	9.21
12	16.01
13	20.37
14	7.59
15	20.14
16	1.73
17	20.14
18	16.74
19	4.24
20	21.31
21	2.73
22	21.20
23	20.65
24	8.15
25	19.36

Note: The relative area is calculated with respect to the total area of the test sample.

exhibiting less than 10% error between model-predicted and measured values. The results of this evaluation are presented in Table 2.

As can be observed in Table 2, the mean value is 12.31%. This demonstrates that even in the absence of precise point identification, the area requiring inspection by alternative methods is considerably reduced. Furthermore, this estimate does not account for non-contiguous low-error regions, which likely represent outliers that can be easily removed, thereby further improving the resolution.

5. Conclusions

The experimental validation demonstrates that although reduction in sensor number leads to degradation in heat source localization capability, the incorporation of simulated test sample behavior effectively mitigates these effects. In the present case, an 11-fold reduction (with a maximum of 25-fold in the worst case) in localization accuracy was observed compared to the ideal configuration with sensors directly positioned at component locations, however this was achieved with a substantially reduced sensor count. Specifically, a sensor-to-component ratio of 5/256 was obtained, corresponding to a 98% reduction in installed sensor quantity. Moreover, the decoupling of the response simulation phase from the identification phase permits optimal execution of each stage independently. The computationally intensive simulation phase can be executed asynchronously relative to the identification phase, which, being computationally lighter, could potentially be implemented directly on the component hardware.

The proposed methodology constitutes a practical strategy for augmenting the spatial resolution of sparse sensor networks, thereby mitigating installation complexity and implementation burden. Furthermore, the synergistic combination of a minimally invasive distributed sensor network with dedicated sensors co-located with mission-critical components enables comprehensive thermal monitoring encompassing both high-priority elements and components typically omitted from conventional monitoring schemes.

References

Buticchi, G., P. Wheeler, and D. Boroyevich (2022). The more-electric aircraft and beyond. *Proceedings of the IEEE 111*(4), 356–370.

Fluchs, S. (2020). The diffusion of electric mobility in the european union and beyond. *Transportation Research Part D: Transport and Environment 86*, 102462.

Kalker, S., L. A. Ruppert, C. H. Van Der Broeck, J. Kuprat, M. Andresen, T. A. Polom, M. Liserre, and R. W. De Doncker (2021). Reviewing thermal-monitoring techniques for smart power modules. *IEEE Journal of Emerging and Selected Topics in Power Electronics 10*(2), 1326–1341.

Kish, L. B. (2002). End of moore's law: thermal (noise) death of integration in micro and nano electronics. *Physics Letters A 305*(3-4), 144–149.

Lakshminarayanan, V. and N. Sriraam (2014). The effect of temperature on the reliability of electronic components. In *2014 IEEE international conference on electronics, computing and communication technologies (CONECCT)*, pp. 1–6. IEEE.

Meijer, G. C., G. Wang, and A. Heidary (2018). Smart temperature sensors and temperature sensor systems. In *Smart Sensors and MEMs*, pp. 57–85. Elsevier.

Rajashekara, K. (2013). Present status and future trends in electric vehicle propulsion technologies. *IEEE journal of emerging and selected topics in power electronics 1*(1), 3–10.

Saito, W. (2023). A future outlook of power devices from the viewpoint of power electronics trends. *IEEE Transactions on Electron Devices 71*(3), 1356–1364.

Theis, T. N. and H.-S. P. Wong (2017). The end of moore's law: A new beginning for information technology. *Computing in science & engineering 19*(2), 41–50.